THE JOURNAL OF PHYSICAL CHEMISTRY C

Article

Cite This: J. Phys. Chem. C 2018, 122, 24823−24829

pubs.acs.org/JPCC

Increasing the Density of Single-Walled Carbon Nanotube Arrays by Multiple Catalysts Reactivation

Zequn Wang,[†,‡] Qiuchen Zhao,[†] and Jin Zhang*[,†]

[†]Center for Nanochemistry, Beijing Science and Engineering Center for Nanocarbons, Beijing National Laboratory for Molecular Sciences, College of Chemistry and Molecular Engineering and [‡]Academy for Advanced Interdisciplinary Studies, Peking University, Beijing 100871, P. R. China

Supporting Information

ABSTRACT: High-density single-walled carbon nanotube (SWNT) array is a basic premise for its application in nanoelectronic devices in the future. Generally, it is considered that the improvement in catalyst efficiency is a possible route to increase the density. Here, we designed a multiple-catalysts reactivation method to increase the catalyst efficiency. By multiple H_2 treatment, we could successfully improve the density of the SWNT arrays by an average of 65%. Moreover, a new model to describe the multiple-catalysts reactivation process was established to deeply understand the mechanism of catalyst poisoning, and two possible types of catalyst poisoning: physical poisoning (PP) and structural poisoning (SP) were proposed. Only poisoned catalysts with PP type could be reactivated to produce new carbon nanotubes. By comparing different metal catalysts, we found that the ratio of PP to SP catalysts was highly related to the growth model, including vapor−solid (VS) and vapor−liquid−solid (VLS) model. Specifically, catalysts with VS mechanism (like W or Cu) showed higher PP ratio than those with VLS mechanism (like Co). The relationship between poisoning type and growth model mode may also contribute to the further catalyst design for high-density SWNT arrays.

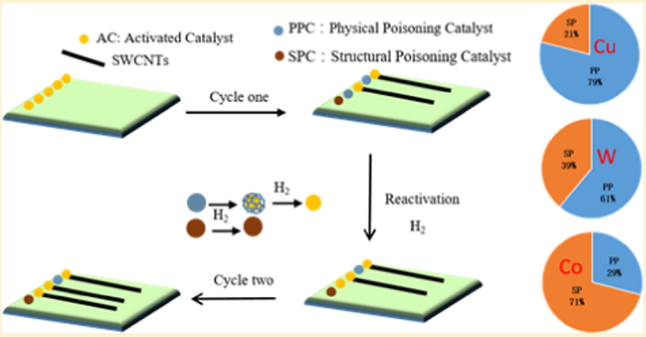

1. INTRODUCTION

The approach to the limit of Moore's law makes researchers eager to search more efficient materials to replace silicon in the semiconducting industry.[1] Single-walled carbon nanotubes (SWNTs) have been regarded as a promising candidate with excellent electronic transport properties.[2] For device applications, high-density horizontally aligned SWNT arrays are intensively required.[3] During the past decade, lots of work has been done to obtain SWNTs with high-density and large scale, including post-treatment method[4−7] and direct growth method.[8,9] In the first approach, the SWNTs were produced in liquid phase after dispersion, such as Langmuir−Schaefer method,[6] fringing-field dielectrophoresis,[4] solution shearing,[7] and Langmuir−Blodgett method,[5] and ion-exchange chemical method.[10] However, the SWNTs inevitably become contaminated, shortened, and misaligned after dispersion in the solution. Meanwhile, great progress has been made on the direct growth method by chemical vapor deposition (CVD) system, which could produce SWNTs with both high quality and high orientation. However, one of the biggest problems that blocks the development of direct growth samples is the low array density. Generally, it is considered that the low density of active catalysts is the reason why the density of SWNTs cannot continue to improve. Therefore, many groups tried to enhance the density of active catalysts by multiple catalysts loading,[11] multiple cycle growth,[12,13] and gradual release of catalysts (which is also called "Trojan Catalysts").[9] The local density of the obtained SWNTs could be as high as 160 tubes per μm by the Trojan Catalyst method on sapphire.[8] Besides simply increasing the amount of loaded catalysts, another way to provide more effective catalysts isto increase the efficiency of the catalysts. Based on this, reactivating the poisoned catalysts is helpful in increasing the opportunity for catalysts to nucleate more SWNTs. Unfortunately, the mechanism of catalyst poisoning is still lacking understanding, blocking further increase in catalyst efficiency.

In this work, we designed a multiple-catalysts reactivation method and carried on the discussion to the poisoning mechanism of the catalysts. Experimentally, we chose H_2 as an etchant to remove the amorphous carbon around the catalysts, which is considered as one of the main reasons for catalyst poisoning. During the experiment, we found that the efficiency of catalysts reactivation decreased with increase in the cycle times, and the reactivation efficiency of different metals was obviously different. We conjectured that there might be different types of catalysts poisoning, which were classified as physical poisoning (PP) and structural poisoning (SP). Only poisoned catalysts with PP type could be reactivated after

Received: August 24, 2018
Revised: October 5, 2018
Published: October 11, 2018

DOI: 10.1021/acs.jpcc.8b08235
J. Phys. Chem. C 2018, 122, 24823−24829

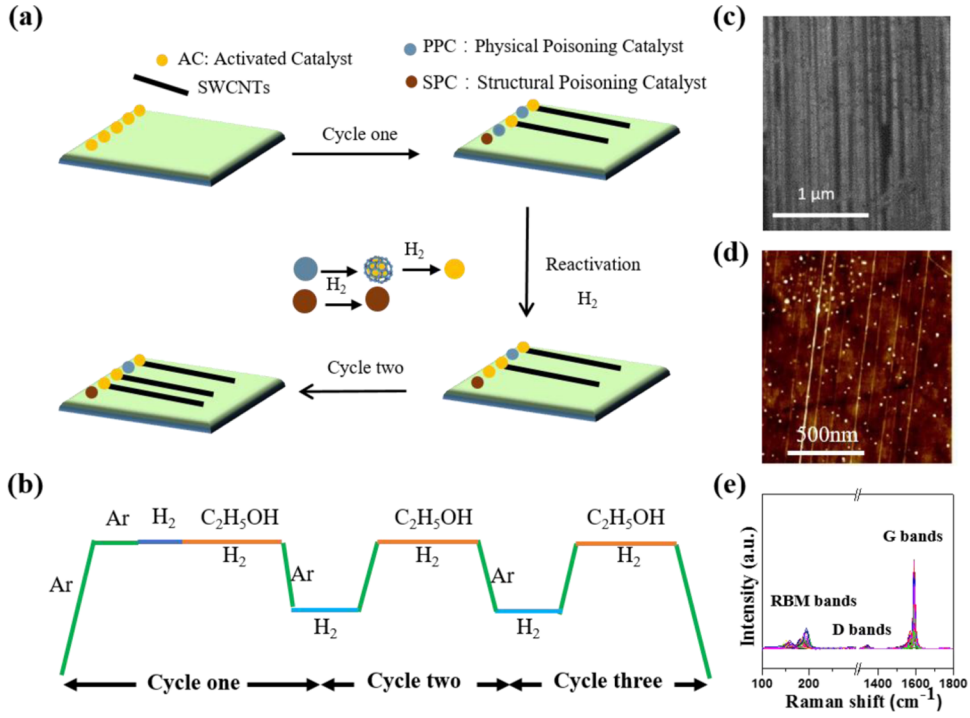

Figure 1. Schematic illustration of multiple-catalysts reactivation process and characterization of SWNT arrays synthesized on quartz. (a) Scheme of growing high-density horizontally aligned SWNT arrays by multiple-catalysts reactivation method. Two different types of catalyst poisoning mode, including physical poisoning and structural poisoning. (b) Experimental process of the growth of SWNT arrays on quartz. (c, d) Scanning electron microscopy (SEM) and atomic force microscopy (AFM) images of the high-density SWNTs on substrate. (e) Raman spectra of the as-grown SWNTs with 514.5 nm excitation.

the hydrogen (H_2) treatment process. Transmission electron microscopy (TEM) and in situ Raman also verified the removal of carbon shells around catalyst nanoparticles, which strongly supported the surmise of PP mechanism. Moreover, we established a new model to describe the multiple-catalysts reactivation process and calculated the probability of catalysts reactivation values of three kinds of metal catalysts. It was found that the ratio of PP to SP catalysts was highly related to the SWNTs growth mode, which could determine the route of carbon species diffusion on the catalysts and further influence the carbon species' deposition and the poisoning of catalysts. Specifically, catalysts with high melting point (like WC) or low carbon solubility (like Cu) trended to follow vapor−solid (VS) mechanism, whereas catalysts with high carbon solubility and lower melting point (like Co) were inclined to follow vapor−liquid−solid (VLS) mechanism. The PP ratio of VS-based catalysts is observed to be much higher than that of VLS-based ones. By using Cu as catalyst, we could improve the density of the SWNT arrays by an average of 65%.

2. METHODS

2.1. Multiple-Catalysts Reactivation Method. The process is illustrated in Figure 1. First, a 4 mm × 6 mm quartz (Hefei Kejing Materials Technology Company, China) was used as substrate for the growth of lattice-oriented SWNT arrays. We scratched catalyst lines on the quartz wafer with $H_{40}N_{10}O_{41}W_{12}$ (0.1 mmol L^{-1}), $CoCl_2$ (0.1 mmol L^{-1}), and $CuCl_2$ (0.1 mmol L^{-1}) ethanol solution by needle and heated the wafer up to 830 °C for 10 min in air. Then, the catalysts were oxidized to W_xO_y, Co_xO_y, and Cu_xO_y respectively. After argon (Ar, >99.99%, 300 sccm) was introduced to eliminate air, H_2 (>99.99%, 50 sccm) was supplied to reduce the catalyst nanoparticle for 10 min. Ethanol, which was used as a carbon source, was introduced afterward into the quartz tube by the bubbling method with Ar as the carrier gas (30−70 sccm). The first growth was finished after 10−30 min. Then, the temperature of the furnace was cooled to 500 °C with Ar (>99.99%, 300 sccm), followed by the introduction of pure H_2 (>99.99%, 50−100 sccm) to reactivate the poisoned catalysts for 15 min. The two steps above are called cycle 1. Next, the furnace temperature was raised to 830 °C with the carbon source and H_2 again, and so on.

2.2. In Situ Catalysts Reactivation Observation Experiments. In situ catalysts reactivation experiments took place by means of miniature CVD system equipped with Raman system. The Raman excitation laser (514 nm) was focused on the sample through a long working distance objective lens (50×). The Raman spectra from 50 to 1800 cm^{-1} were in situ collected per minute in the early stage, and every 10 min from the 10 to 50 min.

2.3. Morphology and Component Characterization of SWNTs. Morphology of SWNT array is characterized by scanning electron microscopy (SEM, Hitachi S4800 field emission, Japan, operated at 1.0 kV), transmission electron microscopy (TEM, FEI Tecnai F30, acceleration voltage 300 kV), and atomic force microscopy (AFM, Dimension icon Scan Asyst). Component characterization of catalysts is characterized by X-ray photoelectron spectroscopy (XPS, Axis Supra/Ultra, 15 kV).

3. RESULTS AND DISCUSSION

3.1. Selection of Etchants and Experimental Design for Catalyst Reactivation Method. To realize the reactivation of poisoned catalysts, it is important to choose a

DOI: 10.1021/acs.jpcc.8b08235
J. Phys. Chem. C 2018, 122, 24823−24829

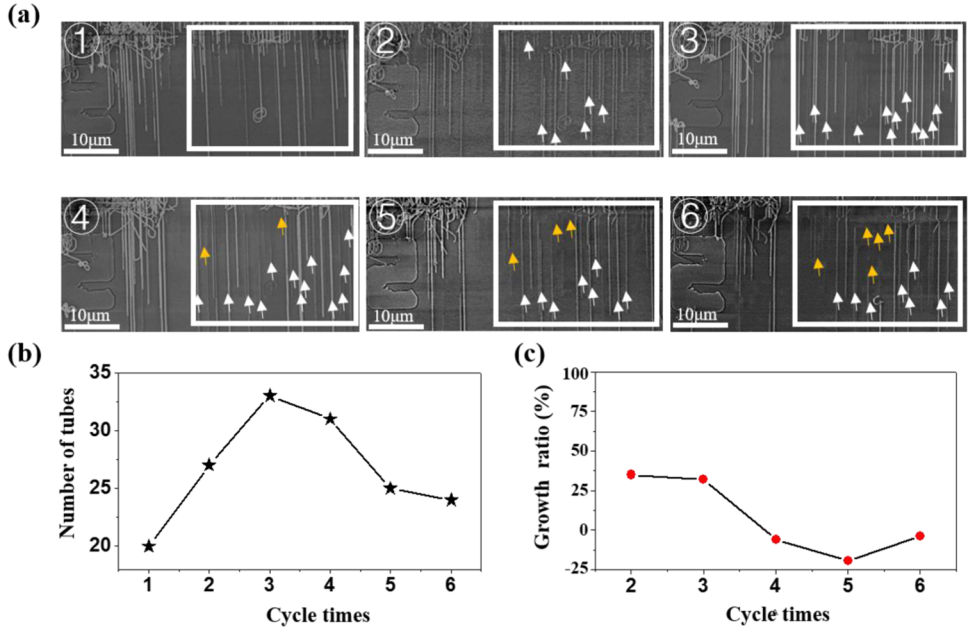

Figure 2. Analysis of the number of tubes and reactivation efficiency during multiple reactivation by Cu. (a) SEM images of SWNTs during multiple reactivation at the same position. Arrows in white refer to the newly grown SWNTs and those in yellow refer to the etched SWNTs. (b) Statistics of the tube numbers over cycle times. (c) Growth ratio of multiple reactivation.

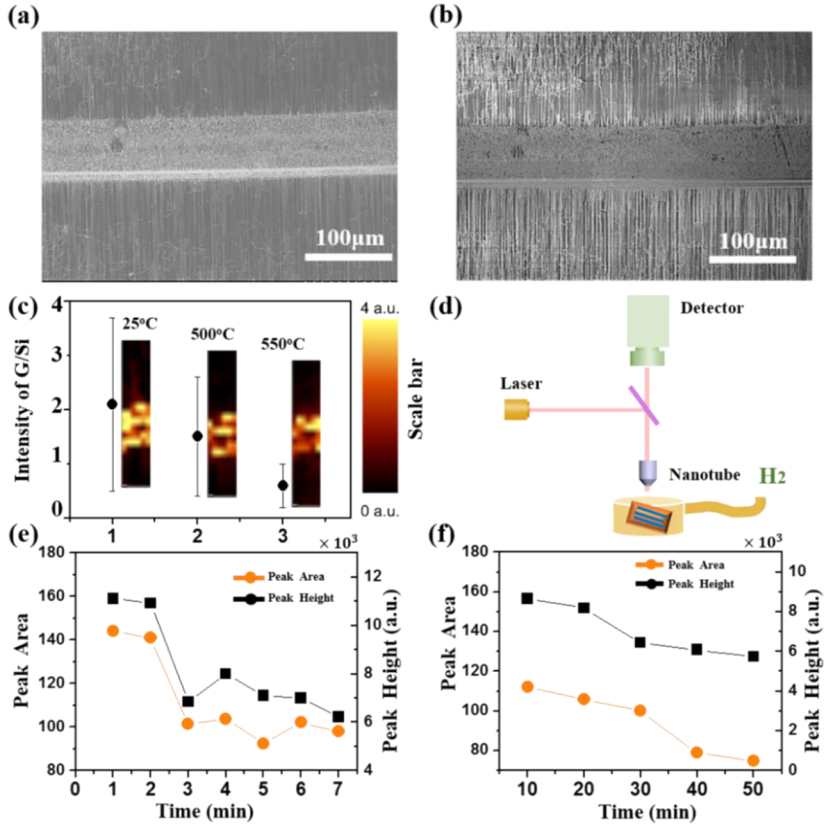

Figure 3. Verification of the effect of the H_2 treatment in the process. (a, b) SEM images of a catalyst strip before (a) and after (b) H_2 treatment. (c) The average intensity and Raman mapping of G-band without H_2 treatment under 25 °C (1) with H_2 treatment under 500 °C (2) and 550 °C (3). The insets are the Raman mapping of the G-band on catalyst stripes by Cu. The wavelength of the excitation laser is 488 nm. (d) The scheme of in situ Raman characterization of the H_2 treatment process. (e) Measurement of the peak area and the peak height from short (e, 1−7 min) and long (f, 10−50 min) periods of time. The wavelength of the excitation laser is 514 nm.

suitable gaseous etchant, such as O_2,[14−16] H_2,[17,18] N_2H_4,[19] H_2O,[20,21] CO_2,[22,23] NH_3,[24] SO_3,[25] etc. Considering that oxidative gases might react with catalysts and form new species,[26] the impact of reductive gases on the structures of

DOI: 10.1021/acs.jpcc.8b08235
J. Phys. Chem. C 2018, 122, 24823−24829

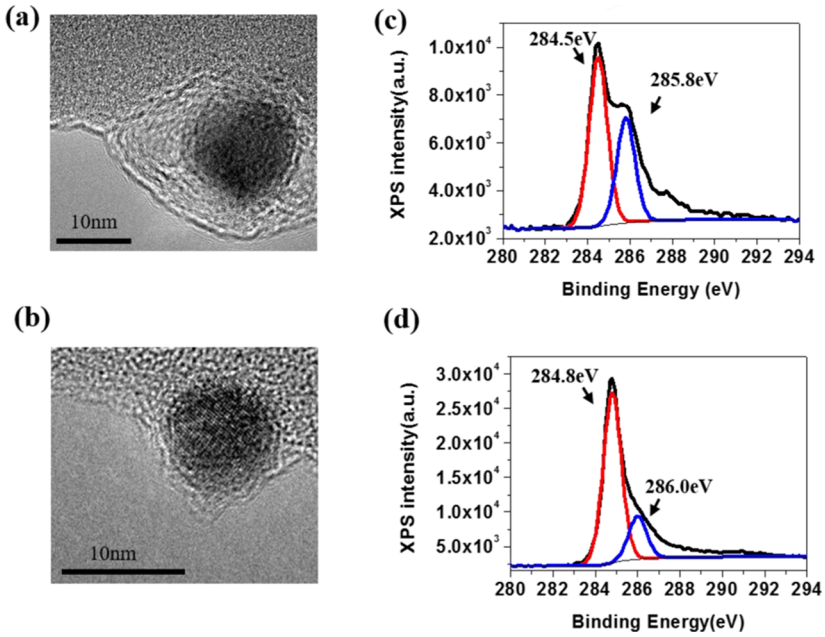

Figure 4. Detailed characterization of catalysts before and after reactivation by Cu. (a, b) TEM characterization of catalysts before (a) and after (b) H_2 treatment. (c, d) XPS characterization of catalysts before (c) and after (d) H_2 treatment.

catalyst might be smaller. Among the reducing etchants, H_2 is widely used in the growth of well-graphitized SWNTs, and adding H_2 for catalysts reactivation could make the system operate easily and continuously.

The schematic illustration of multiple-catalysts reactivation process is shown in Figure 1a,b, and the details of the experimental process are described in Section 2.1. The results show that H_2 could not harm the structure of the SWNTs below 500 °C but could produce fractures on SWNTs above 550 °C (Figure S1). Therefore, we chose 500 °C as a proper temperature for catalysts reactivation in Section 2.1. With this method, we obtained the SWNT arrays with the average density of 18 tubes per μm on quartz (Figure 1c,d). Raman spectra exhibit that the radial breathing peaks were distributed between 160 and 200 cm^{-1}, a strong evidence that our as-grown samples are single-walled with a typical diameter around 1.2−1.6 nm on quartz (d = 248/w). Moreover, the quality of the obtained SWNTs by this method is high, with barely noticeable defect-induced D-band (Figure 1e).

To further analyze the efficiency of catalysts reactivation, we designed six growth cycles by Cu catalysts under the same conditions. Figure 2a demonstrates that the number of SWNTs varies with the growth cycles at the same observation area in which the white arrows in the SEM images refer to the newly grown SWNTs and the yellow ones refer to the etched SWNTs. Figure 2b shows the statistics of the tube numbers over cycle times. We further analyzed the evolution trend of the number of SWNTs and found that the growth ratio was positive in the second growth cycle but turned negative from the fourth growth cycle (Figure 2c), where the growth ratio was defined as the change in the number of SWNTs between adjacent cycles. It indicated that three growth cycles might be the most suitable condition. Overall, the density of SWNT arrays is increased by an average of 65% from one growth cycle to three growth cycles.

We speculated that reactivating and etching effect coexisted in the SWNTs growth process. The reactivating rate of catalysts is higher than the etching rate in the early stage, thus growing effect is dominated. Nevertheless, because the efficiency of catalysts reactivation gradually declines with increase in cycle times, the etching rate will exceed the reactivating rate in the later period. Then, etching effect plays a major role.

3.2. Mechanism of the H_2 Reactivation Process. SEM images show that the SWNTs remain intact (Figure 3a), but catalyst lines become obviously distinct after H_2 etching (Figure 3b). We inferred that the change in the brightness of the catalyst stripes might be caused by the the reduction of electron-rich materials (amorphous carbon, graphitic carbon, etc.) during the H_2 treatment. To find the reason behind this phenomenon, Raman spectroscopy is a useful way to monitor the process with both ex situ and in situ. It is well known that G-band is the tangential mode of sp^2 C−C. Both SWNTs and carbonaceous impurities (graphitic or amorphous carbon particles) would contribute to the G-band intensity. We standardized the intensity of the G-band and calculated the ratio of the G-band to the Si-band, and it was shown that the average intensity of the G/Si ratio on the catalysts strips (data from 48 positions) decreased with increase in the temperature in Figure 3c. Besides, the Raman mapping images of the G-band of catalyst lines without H_2 treatment at room temperature (25 °C) and with H_2 under 500 and 550 °C are shown in the inset. A change in the Raman intensity further improves the disappearance of some of the carbonaceous components on the catalyst region.

In situ observation is helpful for providing the information of the component of catalyst stripes changing over time. Therefore, we proceeded with in situ Raman characterization of the reactivation process by means of miniature CVD system equipped with the Raman system (Figure 3d). Instrument parameters and experimental process are introduced in Section 2.2. The sample is placed on the heating stage at 500 °C and H_2 is supplied throughout the observation process. The Raman signal is collected every minute in the early stage (Figure 3e) and every 10 min from the 10 to 50 min (Figure 3f). The results show that both intensity of the peak area and peak

DOI: 10.1021/acs.jpcc.8b08235
J. Phys. Chem. C 2018, 122, 24823−24829

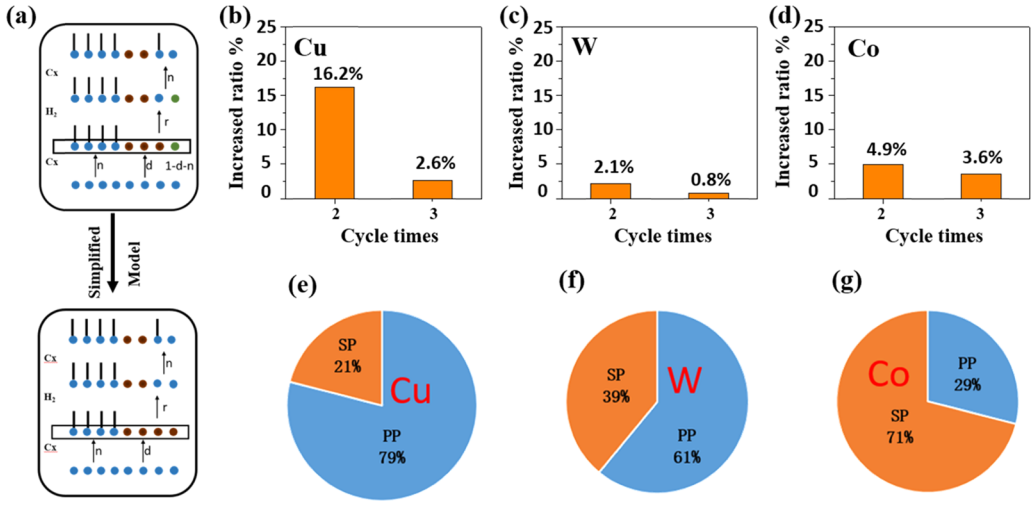

Figure 5. Theoretical model of catalysts reactivation. (a) Schematic illustration of the complicated and simplified growth model for multiple reactivation process. (b–d) Statistics of the growth ratio of SWNTs in the adjacent cycle experiment by using different catalysts of Cu (b), W (c), and Co (d). (e–g) The distribution of the PP and SP of Cu (e), W (f), and Co (g).

height of the G-band decrease significantly over time. The intensity of the Raman signals decreases rapidly in the first several minutes and then becomes slower gradually, which agrees with the classical reaction dynamics.

To provide more intuitive information about the structure of poisoned catalysts and its reactivation, we characterized the morphology of catalyst particles by TEM. We dropped the catalysts solution on the Si_3N_4 grid and put it into the CVD system to grow SWNTs. To improve the possibility to investigate the results of catalysts poisoning, we prolonged the growth time and reactivation time for 1 h. With TEM imaging, it is seen clearly that the surface of the poisoned catalyst particles is overlaid with some continuous laminated materials after one-time growth (Figure 4a). After long-time H_2 treatment, such continuous materials are markedly reduced (Figure 4b). To analyze the chemical component of the materials, we used XPS as a powerful tool. To achieve the lowest detection limit, we changed the substrates and improved the catalysts loading quantity. The result is shown in Figure 4c,d, in which the main peak is 284.5–284.8 eV and the second highest peak is 285.6–286 eV. Because SWNTs are composed of crystallized graphitized layer structures, the main peak is attributed to the graphitic carbon. As for the second highest peak, it is reported to be related to the structural defects on the surface.[27,28] These defects are some carbon atoms in another state beyond pure graphitic sp^2 ones. After the catalysts reactivation, the second highest peak dramatically declined, indicating the amorphous carbon species were removed from the system. Through the above characterization, we claimed that some catalysts could be covered by continuous laminated carbon shells and prevented from further contacting with the carbon feedback, which leads to the inactivation of the catalysts. Moreover, these carbon shells could be etched under our H_2 treatment condition, and catalysts connection is re-established with the carbon feedback. We claimed that the formation of carbon shell should be one of the main mechanisms for catalyst poisoning.

We also found that only part of the poisoned catalysts could be reactivated, and the efficiency of the catalyst reactivation decreased with increase in the cycle times. Based on this, we regarded the poisoned catalysts with reactivation ability as physical poisoning (PP) catalysts and the ones without the reactivation ability as structural poisoning (SP) catalysts. We claimed that carbon shell on the surface of catalysts is the main reason for physical poisoning, whereas the mechanism of structural poisoning is unclear until now. Currently, we speculated that the possible reasons for SP catalysts might be numerous, including Ostwald ripening,[29−31] the migration of the catalysts,[30] transformation into other inactive phases,[32] and so on. It would be helpful to use environmental transmission microscopy to further study the reasons for the structural poisoning catalysts by monitoring the growth process.

3.3. Model of Describing the Multiple-Catalysts Reactivation Process. To compare the ratio of PP catalysts in different metals, we established a growth model to describe the multiple-catalysts reactivation process (Figure 5a). In the initial stage, all of the catalyst particles are active (blue balls). After the first growth, some catalysts lead to the growth of SWNTs (black lines), some catalysts are poisoned (brown balls), and the others keep their catalytic activities (green balls). Then, part of the poisoned catalysts could be reactivated, and some brown balls are transformed into blue balls with a specified probability. After the second growth, newly grown SWNTs are synthesized by the active catalysts, and so on.

For the convenience of description, several parameters are defined, where the total number of the effective active catalysts is N, the probability of catalysts poisoning is d, the probability of catalysts reactivation is r, and the probability of catalyst particles to keep their catalytic activities after one time growth is n, thus the probability of catalysts for SWNTs growth is $1 - d - n$. We assumed that these parameters are constant in the multiple reactivation process. Based on this, the number of SWNTs at different growth cycles (defined as x_1, x_2, x_3,...) is demonstrated by (detailed calculation is shown in Supporting Information, Table S1)

$$\frac{x_2}{x_1} = 1 + (1 - n - d) + dr \quad (1)$$

DOI: 10.1021/acs.jpcc.8b08235
J. Phys. Chem. C 2018, 122, 24823−24829

$$\frac{x_3}{x_1} = 1 + (1 - n - d + dr) \times (1 + 1 - n - d + dr) + dr(1 - r) \quad (2)$$

To further simplify the model, we analyzed the number of SWNTs by Cu catalysts under different growth times (10, 20, 30, and 40 min) in Figure S2 and found that the newly grown SWNTs decreased with increase in growth time. It indicates that if the catalysts particles are provided with sufficient growth time, the active catalysts (including reactivated catalysts) are used either to synthesize new SWNTs or be poisoned. In other words, n can be negligible in eqs 1 and 2. The results show that appropriate growth time for different catalysts is 30 min for Cu, 30 min for Co, and 10 min for W, respectively. Based on this, the simplified model of the number of the SWNTs is shown by (detailed calculation is shown in Supporting Information, Table S2)

$$\frac{x_2}{x_1} = 1 + dr \quad (3)$$

$$\frac{x_3}{x_1} = 1 + dr + dr(1 - r) + d^2r^2 \quad (4)$$

3.4. Efficiency of Reactivation in Different Catalysts.

After a three-cycle reactivation process (including 3 steps of growth and 2 steps of H_2 treatment), we analyzed the difference in the efficiency of reactivation in different catalysts (Cu, W, and Co). Based on the large number of statistical analysis on the increased ratio of SWNTs (defined as $\frac{x_2 - x_1}{x_1}$, $\frac{x_3 - x_2}{x_2}$) in Figure 5b–d, we found that the r in Cu, W, and Co was 0.79, 0.61, and 0.29, respectively. The detailed statistics are illustrated in Figure S3 and Table S3. As discussed above, the probability of poisoned catalysts with reactivation ability is regarded as r, which is also the probability of physical poisoning (PP) catalysts. Only poisoned catalysts with PP type could be reactivated to produce new carbon nanotubes. However, the probability of catalysts without the reactivation ability is regarded as $1 - r$, which is defined as the probability of structural poisoning (SP) catalysts. The results of the distribution of the PP and SP of different catalysts is illustrated in Figure 5e–g, which is 21% SP, 79% PP for Cu, 39% SP, 61% PP for W, and 71% SP, 29% PP for Co.

It is found that the ratio of PP or SP in a kind of catalyst was highly related to the growth model, including vapor–solid (VS) and vapor–liquid–solid (VLS) models. The growth of SWNTs by the VS model is mainly promoted by the surface diffusion of carbon species on the surface of catalysts, and the graphitized initial cap is formed at lower energy state. As for the VLS model, carbon species dissolve into the liquid catalysts and then precipitate to form SWNTs, when the particles are highly supersaturated. Therefore, the growth model could determine the route of carbon species diffusion on the catalysts and further influence the poisoning of catalysts.

Specifically, owing to the low carbon solubility of Cu,[33] SWNTs are grown by a surface-catalyzed process on Cu catalysts, which tend to follow the VS mechanism. The metal–carbon phase diagrams are shown in Figure S4. Meanwhile, because of high melting point, either tungsten or tungsten carbide[34,35] as catalysts are considered to remain solid and stable under the growth process and carbon species migrate on the surface of the catalysts. Thus, W-based catalysts also tend to follow the VS mechanism. The diffusion, migration, and deposition of carbon species mainly happen on the surface of the catalysts,[36] and the treatment of the surface of the catalysts is much more effective. Therefore, this kind of catalysts in the VS mode is easy to be reactivated, which show a high PP ratio (like W or Cu).

Generally, as the melting point of the catalysts is relatively low, Co-based and Fe-based catalysts are considered to be liquid and incline to follow the VLS mechanism.[34] The exchange of the materials between catalysts and carbon species is frequent by the VLS model. Besides, there are newly formed phases during the growth process, for example, Co_3C,[35] Fe_3C, and FeC_x.[3232] The structure and properties of the catalysts are easily changeable, which could easily lead to structural poisoning. Therefore, the effect of the treatment of the surface is limited in this kind of catalysts, which show a high SP ratio (like Co, Fe).

4. CONCLUSIONS

In summary, by multiple-catalysts reactivation, we successfully improved the density of the SWNT array by 65% using Cu catalysts from one growth cycle to three. Furthermore, we built a new model to describe the multiple catalysts reactivation and calculated the probability of catalysts reactivation values of three kinds of metal catalysts (W, Cu, and Co). Based on this, we proposed two possible mechanisms of catalyst poisoning, including physical poisoning (PP) and structural poisoning (SP). And, we found the reactivation efficiency of different metals might be highly related to the growth model, including VLS and VS. The study of the mechanisms of catalyst poisoning and the analysis of the reactivation efficiency may contribute to an improved understanding of catalyst design for high-density SWNT arrays.

■ ASSOCIATED CONTENT

Supporting Information

The Supporting Information is available free of charge on the ACS Publications website at DOI: 10.1021/acs.jpcc.8b08235.

Morphology characterization of SWNTs treated by H_2 under the different temperature; statistics of the increased ratio of the number of SWNTs in different growth times by Cu; the statistics of the increased ratio of the number of the SWNTs by three cycles growth with Cu, Co, and W; detailed calculations about the multiple-catalysts reactivation model; W–C, Co–C, and Cu–C phase diagrams (PDF)

■ AUTHOR INFORMATION

Corresponding Author

*E-mail: jinzhang@pku.edu.cn.

ORCID

Jin Zhang: 0000-0003-3731-8859

Notes

The authors declare no competing financial interest.

■ ACKNOWLEDGMENTS

The authors thank Yue Yu from Peking University for the help of high-resolution TEM images. This work was supported by the Ministry of Science and Technology of China (2016YFA0200101 and 2016YFA0200104), the National Natural Science Foundation of China (grant nos 21233001, 21790052, and 51720105003), and the Beijing Municipal

DOI: 10.1021/acs.jpcc.8b08235
J. Phys. Chem. C 2018, 122, 24823–24829

Science and Technology Planning Project (no. Z161100002116026).

REFERENCES

(1) Waldrop, M. M. The Chips Are Down for Moore's Law. *Nature* **2016**, *530*, 144−147.

(2) Cao, Q.; Han, S.; Tersoff, J.; Franklin, A. D.; Zhu, Y.; Zhang, Z.; Tulevski, G. S.; Tang, J.; Haensch, W. End-Bonded Contacts for Carbon Nanotube Transistors with Low, Size-Independent Resistance. *Science* **2015**, *350*, 68−72.

(3) Franklin, A. D. Electronics: The Road to Carbon Nanotube Transistors. *Nature* **2013**, *498*, 443−444.

(4) Cao, Q.; Han, S.; Tulevski, G. S. Fringing-Field Dielectrophoretic Assembly of Ultrahigh-Density Semiconducting Nanotube Arrays with a Self-Limited Pitch. *Nat. Commun.* **2014**, *5*, No. 5071.

(5) Cao, Q.; Han, S.; Tulevski, G. S.; Zhu, Y.; Lu, D. D.; Haensch, W. Arrays of Single-Walled Carbon Nanotubes with Full Surface Coverage for High-Performance Electronics. *Nat. Nanotechnol.* **2013**, *8*, 180−186.

(6) Islam, A. E.; Rogers, J. A.; Alam, M. A. Recent Progress in Obtaining Semiconducting Single-Walled Carbon Nanotubes for Transistor Applications. *Adv. Mater.* **2015**, *27*, 7908−7937.

(7) Park, S.; Pitner, G.; Giri, G.; Koo, J. H.; Park, J.; Kim, K.; Wang, H.; Sinclair, R.; Wong, H. S. P.; Bao, Z. Large-Area Assembly of Densely Aligned Single-Walled Carbon Nanotubes Using Solution Shearing and Their Application to Field-Effect Transistors. *Adv. Mater.* **2015**, *27*, 2656−2662.

(8) Kang, L.; Hu, Y.; Zhong, H.; Si, J.; Zhang, S.; Zhao, Q.; Lin, J.; Li, Q.; Zhang, Z.; Peng, L.; et al. Large-Area Growth of Ultra-High-Density Single-Walled Carbon Nanotube Arrays on Sapphire Surface. *Nano Res.* **2015**, *8*, 3694−3703.

(9) Hu, Y.; Kang, L.; Zhao, Q.; Zhong, H.; Zhang, S.; Yang, L.; Wang, Z.; Lin, J.; Li, Q.; Zhang, Z.; et al. Growth of High-Density Horizontally Aligned Swnt Arrays Using Trojan Catalysts. *Nat. Commun.* **2015**, *6*, No. 6099.

(10) Park, H.; Afzali, A.; Han, S.; Tulevski, G. S.; Franklin, A. D.; Tersoff, J.; Hannon, J. B.; Haensch, W. High-Density Integration of Carbon Nanotubes Via Chemical Self-Assembly. *Nat. Nanotechnol.* **2012**, *7*, 787−791.

(11) Hong, S. W.; Banks, T.; Rogers, J. A. Improved Density in Aligned Arrays of Single-Walled Carbon Nanotubes by Sequential Chemical Vapor Deposition on Quartz. *Adv. Mater.* **2010**, *22*, 1826−1830.

(12) Zhou, W.; Ding, L.; Yang, S.; Liu, J. Synthesis of High-Density, Large-Diameter, and Aligned Single-Walled Carbon Nanotubes by Multiple-Cycle Growth Methods. *ACS Nano* **2011**, *5*, 3849−3857.

(13) Li, J.; Liu, K.; Liang, S.; Zhou, W.; Pierce, M.; Wang, F.; Peng, L.; Liu, J. Growth of High-Density-Aligned and Semiconducting-Enriched Single-Walled Carbon Nanotubes: Decoupling the Conflict between Density and Selectivity. *ACS Nano* **2014**, *8*, 554−562.

(14) Yu, B.; Hou, P.-X.; Li, F.; Liu, B.; Liu, C.; Cheng, H.-M. Selective Removal of Metallic Single-Walled Carbon Nanotubes by Combined in Situ and Post-Synthesis Oxidation. *Carbon* **2010**, *48*, 2941−2947.

(15) Yu, B.; Liu, C.; Hou, P. X.; Tian, Y.; Li, S.; Liu, B.; Li, F.; Kauppinen, E. I.; Cheng, H. M. Bulk Synthesis of Large Diameter Semiconducting Single-Walled Carbon Nanotubes by Oxygen-Assisted Floating Catalyst Chemical Vapor Deposition. *J. Am Chem. Soc.* **2011**, *133*, 5232−5235.

(16) Zhao, Q.; Yao, F.; Wang, Z.; Deng, S.; Tong, L.; Liu, K.; Zhang, J. Real-Time Observation of Carbon Nanotube Etching Process Using Polarized Optical Microscope. *Adv. Mater.* **2017**, *29*, No. 1701959.

(17) Hou, P.-X.; Li, W.-S.; Zhao, S.-Y.; Li, G.-X.; Shi, C.; Liu, C.; Cheng, H.-M. Preparation of Metallic Single-Wall Carbon Nanotubes by Selective Etching. *ACS Nano* **2014**, *8*, 7156−7162.

(18) Li, W.-S.; Hou, P.-X.; Liu, C.; Sun, D.-M.; Yuan, J.; Zhao, S.-Y.; Yin, L.-C.; Cong, H.; Cheng, H.-M. High-Quality, Highly Concentrated Semiconducting Single-Wall Carbon Nanotubes for Use in Field Effect Transistors and Biosensors. *ACS Nano* **2013**, *7*, 6831−6839.

(19) Pint, C. L.; Kim, S. M.; Stach, E. A.; Hauge, R. H. Rapid and Scalable Reduction of Dense Surface-Supported Metal-Oxide Catalyst with Hydrazine Vapor. *ACS Nano* **2009**, *3*, 1897−1905.

(20) Li, P.; Zhang, J. Sorting out Semiconducting Single-Walled Carbon Nanotube Arrays by Preferential Destruction of Metallic Tubes Using Water. *J. Mater. Chem.* **2011**, *21*, 11815−11821.

(21) Zhou, W.; Zhan, S.; Ding, L.; Liu, J. General Rules for Selective Growth of Enriched Semiconducting Single Walled Carbon Nanotubes with Water Vapor as in Situ Etchant. *J. Am. Chem. Soc.* **2012**, *134*, 14019−14026.

(22) Huang, J.; Zhang, Q.; Zhao, M.; Wei, F. Process Intensification by Co2 for High Quality Carbon Nanotube Forest Growth: Double-Walled Carbon Nanotube Convexity or Single-Walled Carbon Nanotube Bowls? *Nano Res.* **2009**, *2*, 872−881.

(23) Wang, Z.; Zhao, Q.; Tong, L.; Zhang, J. Investigation of Etching Behavior of Single-Walled Carbon Nanotubes Using Different Etchants. *J. Phys. Chem. C* **2017**, *121*, 27655−27663.

(24) Kim, S.; Kim, S.; Lee, H. Effect of Ammonia Gas Etching on Growth of Vertically Aligned Carbon Nanotubes/Nanofibers. *Trans. Nonferrous Met. Soc. China* **2011**, *21*, 130−134.

(25) Zhang, H.; Liu, Y.; Cao, L.; Wei, D.; Wang, Y.; Kajiura, H.; Li, Y.; Noda, K.; Luo, G.; Wang, L.; et al. A Facile, Low-Cost, and Scalable Method of Selective Etching of Semiconducting Single-Walled Carbon Nanotubes by a Gas Reaction. *Adv. Mater.* **2009**, *21*, 813−816.

(26) Warren, A.; Nylund, A.; Olefjord, I. Oxidation of Tungsten and Tungsten Carbide in Dry and Humid Atmospheres. *Int. J. Refract. Met. Hard Mater.* **1996**, *14*, 345−353.

(27) Datsyuk, V.; Guerretpiecourt, C.; Dagreou, S.; Billon, L.; Dupin, J.; Flahaut, E.; Peigney, A.; Laurent, C. Double Walled Carbon Nanotube/Polymer Composites Via in-Situ Nitroxide Mediated Polymerisation of Amphiphilic Block Copolymers. *Carbon* **2005**, *43*, 855−894.

(28) Datsyuk, V.; Kalyva, M.; Papagelis, K.; Parthenios, J.; Tasis, D.; Siokou, A.; Kallitsis, I.; Galiotis, C. Chemical Oxidation of Multiwalled Carbon Nanotubes. *Carbon* **2008**, *46*, 833−840.

(29) Kim, S. M.; Pint, C. L.; Amama, P. B.; Hauge, R. H.; Maruyama, B.; Stach, E. A. Catalyst and Catalyst Support Morphology Evolution in Single-Walled Carbon Nanotube Supergrowth: Growth Deceleration and Termination. *J. Mater. Res.* **2010**, *25*, 1875−1885.

(30) Kim, S. M.; Pint, C. L.; Amama, P. B.; Zakharov, D. N.; Hauge, R. H.; Maruyama, B.; Stach, E. A. Evolution in Catalyst Morphology Leads to Carbon Nanotube Growth Termination. *J. Phys. Chem. Lett.* **2010**, *1*, 918−922.

(31) Amama, P. B.; Pint, C. L.; Mcjilton, L.; Kim, S. M.; Stach, E. A.; Murray, P. T.; Hauge, R. H.; Maruyama, B. Role of Water in Super Growth of Single-Walled Carbon Nanotube Carpets. *Nano Lett.* **2009**, *9*, 44−49.

(32) Harutyunyan, A. R.; Awasthi, N.; Jiang, A.; Setyawan, W.; Mora, E.; Tokune, T.; Bolton, K.; Curtarolo, S. Reduced Carbon Solubility in Fe Nanoclusters and Implications for the Growth of Single-Walled Carbon Nanotubes. *Phys. Rev. Lett.* **2008**, *100*, 195502.

(33) López, G. A.; Mittemeijer, E. J. The Solubility of C in Solid Cu. *Scr. Mater.* **2004**, *51*, 1−5.

(34) Zhang, S.; Kang, L.; Wang, X.; Tong, L.; Yang, L.; Wang, Z.; Qi, K.; Deng, S.; Li, Q.; Bai, X.; et al. Arrays of Horizontal Carbon Nanotubes of Controlled Chirality Grown Using Designed Catalysts. *Nature* **2017**, *543*, 234−238.

(35) Landois, P.; Peigney, A.; Laurent, C.; Frin, L.; Datas, L.; Flahaut, E. CCVD Synthesis of Carbon Nanotubes with W/Co−Mgo Catalysts. *Carbon* **2009**, *47*, 789−794.

(36) Li, X.; Cai, W.; An, J.; Kim, S.; Nah, J.; Yang, D.; Piner, R. D.; Velamakanni, A.; Jung, I.; Tutuc, E.; et al. Large-Area Synthesis of High-Quality and Uniform Graphene Films on Copper Foils. *Science* **2009**, *324*, 1312−1314.

DOI: 10.1021/acs.jpcc.8b08235
J. Phys. Chem. C 2018, 122, 24823−24829